Structure and local reactivity of the Au(111) surface reconstruction

Felix Hanke and Jonas Björk

Linköping University Post Print

Structure and local reactivity of the Au(111) surface reconstruction

Felix Hanke[*]

Surface Science Research Centre and Department of Chemistry, University of Liverpool, Oxford Street, Liverpool L69 3BX, United Kingdom

Jonas Björk

Department of Physics, Chemistry and Biology, IFM, Linköping University, 58183 Linköping, Sweden

The close-packed (111) surface of gold is well known to show a $22 \times \sqrt{3}$ reconstruction on single nm lengths with a long-range herringbone pattern on scales of a few hundred nm. Here we investigate the local reconstruction using density functional theory and compare the results to scanning tunneling microscopy experiments. Moreover, we use hydrogen and fluorine as probe atoms to investigate changes in the ability of the Au(111) surface to catalyze the reactions involved in the formation of molecular nanostructures. We find a small variation of the reactivity across different surface sites and link those results to the local coordination environment of the face-centered-cubic (fcc), hexagonal-close-packed (hcp), and ridge regions. Finally, we scrutinize a commonly used approximation in density functional studies, namely that Au(111) is atomically flat and a perfect termination of the fcc lattice.

I. INTRODUCTION

Solid gold is one of the most chemically inert substances and is known to remain pristine and shiny in jewelry, religious statues, and ornate architecture designed to last millennia. At the same time, gold nanoparticles are known to be very reactive and make excellent catalysts for a wide variety of substances.[1–5] These apparently contradictory properties of the same material are at the heart of an active research field in current surface science. While pristine Au surfaces are unable to dissociate hydrogen and oxygen molecules,[2,6] they significantly lower the temperature for dehalogenation reactions that are an important step in the assembly of covalently bonded molecular nanostructures[7–11] and graphene nanoribbons.[12,13]

To modify chemical bonds bonds in these surface science applications, one requires a relatively chemically inert surface to which large molecules adhere primarily through noncovalent van der Waals interactions, yet one that is reactive enough to cleave only a few bonds. Au(111) has technical advantages in that it is relatively easy to obtain a clean atomically flat surface. Its unique reconstruction has been characterized experimentally using scanning tunneling microscopy (STM)[14–18] and other surface science techniques,[19–22] and a large number of molecular assembly studies have been performed on this surface.[7,12,23–28]

The renewed interest in the chemical reactivity on the Au(111) surface is intricately linked to its atomic-level surface structure and its reconstruction, and provides a significant challenge to modern electronic structure theory. In fact, most density functional computational studies make the approximation that Au(111) is an infinite, perfect, atomically flat close-packed face-centered-cubic (fcc) surface. Here we use density functional theory to investigate the detailed atomic arrangement of the reconstruction underlying the characteristic herringbone pattern. In particular, we discuss the role and the degree of influence of the corrugation on the chemisorption of atomic species. Given the changes in the atomic coordination across the reconstructed surface, we investigate to what extent the various surface sites show changes in their reactivity.

Using Fig. 1, we first provide an overview of the herringbone reconstruction. The basic unit cell is two atomic rows wide in the ⟨112⟩ direction and contains two extra atoms every 22 lattice spacings in the ⟨110⟩ surface direction (in a $22 \times \sqrt{3}$ unit cell). The unit cell contains 44 and 46 atoms in the bulk and in the surface layer, respectively.[16,19] The top layer is compressed by 4.34% in the close-packed ⟨110⟩ direction, such that the atoms line up with different sites on layers beneath the surface; see Fig. 1(a).

A large portion of the surface can be associated with an fcc top-layer alignment, while a smaller fraction aligns mostly with hexagonal-close-packed (hcp) surface sites. In addition, the overoccupation and compression leads to a slight buckling of the top Au layer between the two separate fcc and hcp regions. The resulting straight ridges are obvious features in any STM image of a clean reconstructed Au(111) surface and are clearly visible in Fig. 1(b).

To understand the atomic and electronic structure of the Au(111) surface computationally, we focus on a characterization of the straight sections in the herringbone reconstruction using density functional theory (DFT). A similar study on the incommensurate reconstruction of the Au(100)[30] surface has recently shown the utility of such an approach in understanding the origin of the surface structure. Previous theoretical and computational work on the Au(111) surface has included one density functional study[31] which was not able to resolve the difference between hcp and fcc surface regions, as well as work using embedded atom potentials,[32,33] and approximate treatments using Frenkel-Kontorova models for the effective surface potential.[34,35] However, none of these studies provided an explicit discussion of both atomistic and electronic degrees of freedom of the surface.

II. COMPUTATIONAL METHODS

Our DFT calculations were performed using the VASP computational package.[36,37] With applications to largely physisorbed molecular nanostructures in mind, we use the van der Waals density functional (vdWDF)[38,39] with the
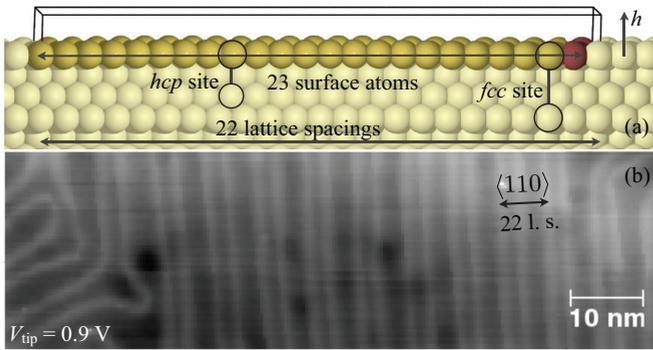
FIG. 1. (Color online) (a) Schematic representation of the Au(111)/$22 \times \sqrt{3}$ reconstruction, showing how 23 surface atoms fit into 22 lattice sites by compressing the top layer of the surface with the additional atoms colored dark red. The positions corresponding to lined-up fcc and hcp sites are indicated by the vertical lines. (b) STM image of the Au(111) herringbone reconstruction ($V_{\text{tip}} = 0.9$ eV, $I_{\text{set}} = 1$ nA; Ref. 29).

Perdew-Burke-Ernzerhof (PBE) exchange functional,[40] which is frequently being used to describe the adsorption of organic molecules on metal surfaces.[41–46] This functional is denoted as vdWDF/PBE. Key results were also calculated using the PBE generalized-gradient approximation.[40] Our plane-wave cutoff has been fixed at 400 eV, which was found to provide an accurate description of the ideal Au surface. The Brillouin sampling was performed using Monkhorst-Pack grids, determined such that the k-point spacing Δk is related to its corresponding lattice vector length ℓ via $\ell \Delta k \geqslant 40$. This gives a k grid of $15 \times 15 \times 15$ for a single atom bulk unit cell, $1 \times 8 \times 1$ for the $22 \times \sqrt{3}$ surface unit cell, and $5 \times 5 \times 1$ for an ideal 3×3 surface cell. In each surface calculation, the periodic images of the slab were separated by 20 Å vacuum. Except for convergence calculations, all unit cells have six layers of Au atoms for which the top four layers are optimized and the bottom two layers remain frozen in their bulk position. This amounts to 266 Au atoms in the fully reconstructed unit cell. The optimized lattice constants for the two functionals are 4.238 and 4.176 Å for vdwDF/PBE and PBE respectively.

III. LOCAL STRUCTURE OF THE $22 \times \sqrt{3}$ RECONSTRUCTION

Using our results for the optimized surface cell[47] as described in Fig. 1, the net energy gain due to the reconstruction is calculated as

$$\Delta E_{\text{Au}(111)} = E_{22 \times \sqrt{3}} - 44 E_{1 \times 1, \text{ideal}} - 2 E_{\text{Au,bulk}}, \quad (1)$$

where $E_{22 \times \sqrt{3}}$ is the total energy of the reconstructed and relaxed six-layer slab, $E_{1 \times 1, \text{ideal}}$ is the energy of an ideal 1×1 six-layer surface cell, and $E_{\text{Au,bulk}}$ is the total energy of a Au atom in the bulk. The bulk energy reference was chosen for the most stable Au atoms available in the crystal, such that our result provides a lower estimate for the actual surface stability. For one $22 \times \sqrt{3}$ unit cell, this calculation gives a reconstruction energy gain of 1.14 (1.10) eV per unit cell, or 25 (24) meV per top-layer atom for vdWDF/PBE (PBE). Our density functional calculation does indeed predict a very
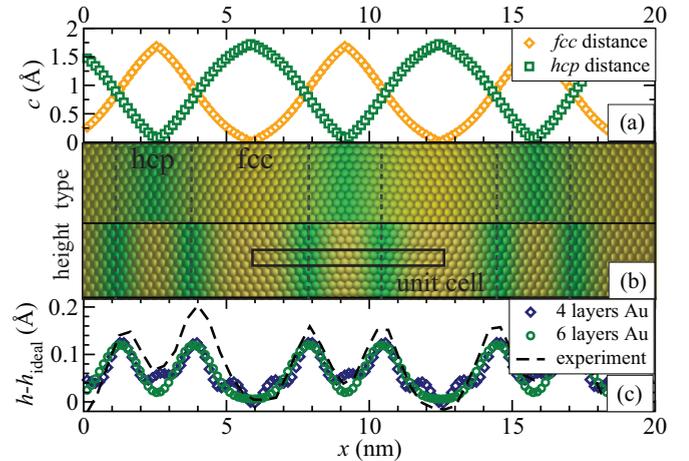

FIG. 2. (Color online) Calculated structure of the reconstructed Au(111) surface, using the vdWDF/PBE density functional. (a) Site character c: distance from the ideal fcc and hcp site for each atom in the top layer, as discussed in the text. (b) Structure of the top layer. The color coding in the top half denotes the atom type, with yellow atoms being of fcc and green atoms being of hcp type. On the bottom half, the color indicates atomic height, with yellow atoms being the closest to the ideal fcc lattice continuation from below. (c) Calculated top-layer height with respect to the ideal fcc lattice and an experimental line scan (Ref. 29).

stable reconstruction with respect to the perfect fcc surface. Our values derived for six-layer slabs are significantly higher than the 0.43 eV/unit cell (9 meV/surface atom) obtained in a previous calculation[31] for a PBE calculation on three layers Au. A separate calculation of a four-layer slab with vdWDF/PBE resulted in a reconstruction energy gain of 1.95 eV per unit cell (42 meV/surface atom); however, we show below that four layers are likely to be insufficient for a reasonable geometric and electronic description of the reconstruction.

In Fig. 2, we present the calculated structure of the reconstructed surface and different measurements taken on the top-layer atoms from the vdWDF/PBE calculation.[47] The atomic coordinates for a single unit cell are provided in the supporting information. The top panel in Fig. 2 displays the site *character* of the surface atoms in Fig. 2(a), also color-coded into the top half of Fig. 2(b). This character c is described by the horizontal (i.e., in-plane) distance from the nearest fcc and hcp site. Top-layer atoms are assigned to the fcc region, when they are closer to the nearest fcc than the next hcp site, and vice versa. Using this assignment, the fcc and hcp regions have widths of 38 and 28 Å respectively. This measurement is consistent with the experimental observation that the fcc region is significantly larger than the hcp region.[16] However, the data in Fig. 2 also show that the site alignment is a continuous and slowly varying function of the distance across the reconstruction and that the perfectly lined-up fcc and hcp regions are at most 2–3 atoms wide for each part of the reconstruction.

The height of each top-layer atom is described by its deviation from the height of an ideal fcc surface termination. It is shown in Fig. 2(c) and color-coded into the bottom half of Fig. 2(b). The graph shows a comparison between the calculated height for a six-layer slab, the calculated height for
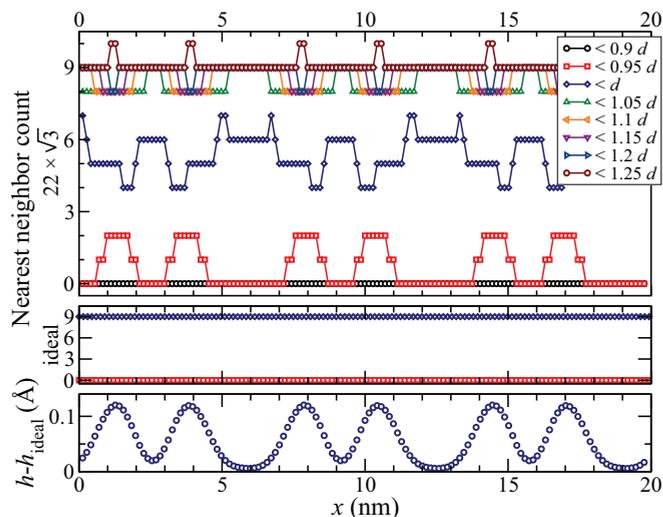
FIG. 3. (Color online) Top: Nearest neighbor (NN) distribution for the top layer of the reconstructed Au surface. Shown are the number of neighboring atoms located within the distances shown in the legend, where d is the bulk NN spacing. (middle) In the ideally terminated fcc surface, the nearest-neighbor count shows a uniform surface coordination. Bottom: The top-layer height profile for our six-layer calculation as in Fig. 2 is provided for reference.

a four-layer slab, and a measured STM line profile—showing a good match between theoretical prediction and experiment for the six-layer slab.

These calculations also demonstrate the necessity to use more than four atomic layers to obtain a fully converged structure. Our four-layer calculation was unable to obtain the smooth top-layer profile visible in STM images, and instead shows a triple-minimum of the height in the fcc region [see Fig. 2(c)]. We attribute this triple minimum to the insufficiently relaxed subsurface layers, which are restricted by the fixed bottom two layers in the four-layer cell. Note that this triple minimum is also visible in STM simulations (shown in Supplemental Material[47]).

Our calculations on the six-layer slab show that the first subsurface atomic layer still contains height variations of up to 0.035 Å. We would like to point out the good match between the calculated ridges in the height profiles and the crossover between fcc and hcp surface regions shown in Fig. 2. The highest surface atoms correspond to the greatest mismatch between the top layer and the underlying surface. We will return to this point when discussing the electronic structure of the surface in the next section.

The last structural feature to investigate is the variation of the surface atom coordination. This information is helpful to assess and understand the reactivity of the different regions of the $22 \times \sqrt{3}$ unit cell. Figure 3 shows the number of adjacent atoms within a certain distance of each surface atom, again for vdWDF/PBE. Here, d is the bulk nearest-neighbor spacing. For an ideal geometry-optimized fcc surface, this coordination plot should be zero for up to the distance d, and then exactly 9 just below the second-nearest neighbor spacing (i.e., Fig. 3 middle).

The key result from this analysis is that large portions of the top layer are slightly *less* coordinated than the ideal

Au(111) surface. While there are a few top-layer atoms that have neighbors at distances as close as 95% of the ideal nearest-neighbor spacing, the ideal coordination number of 9 is reached only for distances between $1.1d$ in the fcc and hcp regions, and $1.25d$ in the ridge region. This phenomenon is due to the symmetric nature of the bulk-terminated surface. A relatively small lateral compression of 4.34% as it is seen in the $22 \times \sqrt{3}$ reconstruction requires most of the surface atoms to sit away from the high-symmetry sites of the underlying lattice, which slightly reduces their coordination. A comparison between vdWDF/PBE and PBE (shown in Supplemental Material[47]) shows that the vdWDF/PBE predicts a marginally more open surface but is otherwise very similar.

IV. SURFACE ELECTRONIC STRUCTURE AND REACTIVITY

To investigate the electronic structure of the reconstructed Au(111) surface, we use two different techniques. Primarily, we are interested in adsorption, which is important for the surface's ability to catalyze chemical reactions. To this extent, we use the adsorption energy of probe atoms optimized on all hollow sites while keeping the surface atoms fixed. Hydrogen is the simplest atom for this purpose and is a classic example for studying the structure and reactivity of different metal surfaces, having been used to demonstrate that *gold is the noblest of all metals*.[6] However, owing to its partially filled antibonding orbital,[6] the energy minimum obtained from H adsorption on Au is only metastable, and the overall interaction is repulsive with respect to the bare Au surface and H_2 in the gas phase. In addition, only the occupied states around 8 eV below the Fermi level are probed (see Supplemental Material[47]).

To select a second probe atom, we remember that carbon-halogen bonds dissociate on the Au(111) surface at elevated temperatures, and that these reactions are catalyzed by the surface.[7,9,10,12] We therefore use a halogen as a second probe, which also probes a higher energy range in the occupied states of Au(111). According to our preliminary calculations on the ideal surface, all halogens cover the same energy range in the density of states,[47] therefore we use the smallest halogen— fluorine—for the current study.

The adsorption energies of these two probe atoms on different sections of the Au(111) reconstruction can be used as a probe for the local reactivity[48,49] of the surface, particularly during the formation of covalently coupled molecular nanostructures. Similar to the atomic coordination-driven contrast in catalytic activity between solid gold and the Au nanoparticles, these energies measure both the local coordination and local electronic structure changes across the reconstruction.

Figure 4 shows the results for the adsorption of both H (top) and F (middle) probe atoms on a frozen substrate, calculated for all possible hollow sites available on the surface. The surface reconstruction height is again shown for reference in the bottom panel. From the top two panels, it is apparent that the calculated probe atom energies do follow the reconstruction and change by up to 45 and 60 meV for the hydrogen and fluorine probes respectively. This calculation demonstrates the possible influence of the surface position on the adsorption behavior. We also see the well known effect that the adsorption
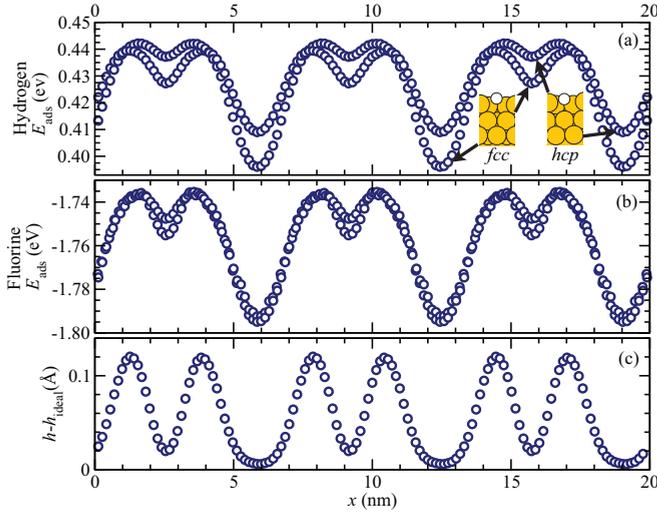
FIG. 4. (Color online) Energies of H (a) and F (b) atoms adsorbed on the frozen Au(111) surface. The two types of hollow site are clearly distinguishable in both fcc and hcp region for H adsorption, while only a small difference in the hcp site type is observed for F adsorption. (c) The surface atom height profile is repeated from Fig. 2(c).

FIG. 5. (Color online) The symbols show the position of the integrated d-band centers with respect to the Fermi level for all atoms in the six-layer Au $22 \times \sqrt{3}$ unit cell according to Eq. (2). The bottom two layers have been kept fixed as indicated by the parentheses in the legend. Each layer has a correspondingly colored dashed line which indicates the equivalent position of the d-band center for an unreconstructed unit cell. The thick solid line shows the d-band center for bulk gold.

energy changes slightly when moving between fcc and hcp hollow sites. As indicated schematically in Fig. 4(a), the effect is somewhat more significant for hydrogen probes and barely visible for fluorine [Fig. 4(b)]. However, it is important to note that the change between adsorption site is significantly less important than the position on the reconstruction.

Placing hydrogen (fluorine) probes on an unreconstructed frozen Au(111) surface results in interaction energies of 0.343 (−1.855) and 0.373 (−1.849) eV for fcc and hcp hollow sites respectively. When comparing these numbers with those presented in Fig. 4, we see that the unreconstructed surface appears to systematically interact more strongly with the adatoms than the reconstructed surface. This effect is comparable to the overall change in energy across the reconstruction, particularly for the more stable fcc site. Our observation could become important in situation where high-accuracy determinations of adsorption energies are essential.

Note that the substrate was kept frozen in these calculations to investigate the electronic effects of the probe atoms rather than the slight structural relaxations around the adsorbate. To test the changes of fully optimized adsorption energies across the reconstruction, three test calculations were performed with H atoms located on the fcc, hcp, and ridge regions. These fully optimized calculations showed that the energy decreases by an amount between about 53–65 meV, irrespective of whether this relaxation was done on the fcc or hcp regions or on the ridge region.

Inspired by the d-band model for surface reactivity,[6,50] we derive a second indicator of local reactivity from the atom-resolved partial density of states, which is presented in Fig. 5. By calculating the central moment of the projected density of the Au $5d$ states ($g_{PDOS,5d}$), we obtain an approximate yet insightful picture of how the electronic structure changes across the entire unit cell as a function of the position and for different atomic layers. These integrals are calculated from the
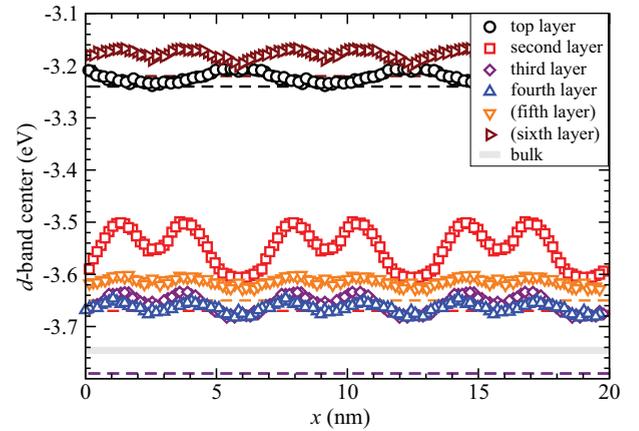
equation

$$\langle E_d \rangle = \frac{\int dE \, E g_{PDOS,5d}}{\int dE \, g_{PDOS,5d}}, \tag{2}$$

and can be visualized as a measure for the center of the d states of each atom. We realize this atom-resolved integration over the entire projected density of states in the d band is a significant approximation of the surface band structure. However, as discussed below, this way we are able to obtain qualitative information about both the surface structure and its reactivity that would otherwise be very difficult to access.

The most striking result found in Fig. 5 is that the most significant changes in the d states are in the second atomic layer, while the top layer hardly changes at all across the reconstruction. Moreover, the location of the second-layer d states exactly mirrors the adsorption energy as well as the height profiles. We explain this phenomenon with the vacuum-level quenching of the states associated with the top-layer atoms. This interpretation is consistent with the top-layer d states being significantly higher than the other atomic layers. Moreover, the top-layer d states are also approximately at the same energetic position as those of the frozen bottom surface layer of gold.

Figure 5 also allows a comparison with the bulk d-band center, which is located near the position of the third and fourth layer's d states in our six-layer cell. This analysis further highlights an electronic structure reason to use more than four atomic layers: In a four-layer cell, the electronically most perturbed second layer would also be the innermost layer and could not very well be taken as a reasonable approximation of bulk gold, which is necessary for the customary supercell approximation to work.

Lastly, we can use Fig. 5 to explain why the experimental profile of the STM line scan is so remarkably well represented with the height profile of our surface unit cell. It is well known that the STM signal is the result of overlapping electronic states

between the tip and sample, where the tip height is adjusted to keep the tunneling current constant. The measured surface height is a convolution of the physical height of the atoms combined with any perturbations of the electronic structure several angstroms above the surface. From Fig. 5, we see that the states associated with the top layer appear to be relatively uniform across the reconstruction. Therfore, it is likely that the net electronic perturbation visible in scanning tunneling microscopy is very small and that the measured height profile is almost entirely due to the physical perturbation of the surface.

V. CONCLUSION

In summary, we have performed extensive electronic structure calculations on the $22 \times \sqrt{3}$ reconstruction of the Au(111) surface using density functional theory. We elucidate the details of the atomic structure, in particular the form and width of the fcc, hcp, and ridge regions of this reconstruction which give rise to the characteristic herringbone pattern seen in scanning tunneling microscopy.

We analyze the local coordination of the surface atoms and show how small differences in the coordination and the local electronic structure give rise to changes in the local reactivity of different surface regions that are also reflected in the subsurface electronic structure. These small variations in the reactivity provide a link to the apparent discrepancy between the chemical inertness of solid gold and the high catalytic activity of gold nanoclusters. The ridge regions, which are undercoordinated in comparison to the perfect fcc and hcp regions, are also found to have slightly less stable adsorption energies.

The original starting point of this study was a question question frequently asked by experimentalists, namely how important it is that density functional studies on the Au(111) surface most often neglect its reconstruction. We find that this approximation potentially overestimates the computed interaction energies, but that the changes involved appear to be well below 100 meV for a single chemisorption bond. In most cases, this difference is unlikely to yield any qualitative physical changes. However, the awkwardly sized reconstruction could become important in situations where the exact location of the adsorbate on the substrate does make a difference and where a high-quality description of adsorption is essential.

Finally, we note that this work was limited only to the straight regions of the reconstructed Au(111) surface. Owing to system size limitations, we were unable to study the elbow sites which are very important in the characteristic herringbone reconstruction. The atomic structure on these elbow sites is expected to be much more open, which would make the analysis of local reactivity and electronic structure all the more interesting.

*Now at Accelrys, 334 Science Park, Cambridge, CB4 0WN, United Kingdom; felix.hanke@accelrys.com

[1] M. Haruta and M. Daté, Appl. Catal. A: Gen. **222**, 427 (2001).

[2] M. Haruta, CATTECH **6**, 102 (2002).

[3] L. Barrio, P. Liu, J. A. Rodríguez, J. M. Campos-Martín, and J. L. G. Fierro, J. Chem. Phys. **125**, 164715 (2006).

[4] T. Fujitani, I. Nakamura, T. Akita, M. Okumura, and M. Haruta, Angew. Chem. Int. Ed. **48**, 9515 (2009).

[5] A. Zanchet, A. Dorta-Urra, O. Roncero, F. Flores, C. Tablero, M. Paniagua, and A. Aguado, Phys. Chem. Chem. Phys. **11**, 10122 (2009).

[6] B. Hammer and J. K. Nørskov, Nature **376**, 238 (1995).

[7] L. Grill, M. Dyer, L. Lafferentz, M. Persson, M. V. Peters, and S. Hecht, Nat. Nanotechnol. **2**, 687 (2007).

[8] M. Bieri, M.-T. Nguyen, O. Gröning, J. Cai, M. Treier, K. Aït-Mansour, P. Ruffieux, C. A. Pignedoli, D. Passerone, M. Kastler, K. Müllen, and R. Fasel, J. Am. Chem. Soc. **132**, 16669 (2010).

[9] L. Lafferentz, V. Eberhardt, C. Dri, C. Africh, F. Esch, S. Hecht, and L. Grill, Nat. Chem. **4**, 215 (2012).

[10] A. Saywell, J. Schwarz, S. Hecht, and L. Grill, Angew. Chem. Int. Ed. **51**, 5096 (2012).

[11] J. Björk, F. Hanke, and S. Stafström, J. Am. Chem. Soc. **135**, 5768 (2013).

[12] J. Cai, P. Ruffieux, R. Jaafar, M. Bieri, T. Braun, S. Blankenburg, M. Muoth, A. P. Seitsonen, M. Saleh, X. Feng, K. Müllen, and R. Fasel, Nature (London) **466**, 470 (2010).

[13] J. Björk, S. Stafström, and F. Hanke, J. Am. Chem. Soc. **133**, 14884 (2011).

[14] R. C. Jaklevic and L. Elie, Phys. Rev. Lett. **60**, 120 (1988).

[15] M. M. Dovek, C. A. Lang, J. Nogami, and C. F. Quate, Phys. Rev. B **40**, 11973 (1989).

[16] J. V. Barth, H. Brune, G. Ertl, and R. J. Behm, Phys. Rev. B **42**, 9307 (1990).

[17] Y. Hasegawa and P. Avouris, Science **258**, 1763 (1992).

[18] H. Y. Nie, W. Mizutani, and H. Tokumoto, Surf. Sci. **311**, L649 (1994).

[19] M. A. Van Hove, R. J. Koestner, P. C. Stair, J. P. Biberian, L. L. Kesmodel, I. Bartos, and G. A. Somorjai, Surf. Sci. **103**, 189 (1981).

[20] U. Harten, A. M. Lahee, J. P. Toennies, and C. Wöll, Phys. Rev. Lett. **54**, 2619 (1985).

[21] K. G. Huang, D. Gibbs, D. M. Zehner, A. R. Sandy, and S. G. J. Mochrie, Phys. Rev. Lett. **65**, 3313 (1990).

[22] A. R. Sandy, S. G. J. Mochrie, D. M. Zehner, K. G. Huang, and D. Gibbs, Phys. Rev. B **43**, 4667 (1991).

[23] N. J. Tao, J. A. DeRose, and S. M. Lindsay, J. Phys. Chem. **97**, 910 (1993).

[24] T. Yokoyama, S. Yokoyama, T. Kamikado, Y. Okuno, and S. Mashiko, Nature (London) **413**, 619 (2001).

[25] L. M. A. Perdigaõ, E. W. Perkins, J. Ma, P. A. Staniec, B. L. Rogers, N. R. Champness, and P. H. Beton, J. Phys. Chem. B **110**, 12539 (2006).

[26] P. A. Staniec, L. Perdigão, A. Saywell, N. R. Champness, and P. H. Beton, Chem. Phys. Chem. **8**, 2177 (2007).

[27] L. Lafferentz, F. Ample, H. Yu, S. Hecht, C. Joachim, and L. Grill, Science **323**, 1193 (2009).

[28] M. Treier, C. Pignedoli, T. Laino, R. Rieger, K. Müllen, D. Passerone, and R. Fasel, Nat. Chem. **3**, 61 (2010).

[29] LT-UHV-STM data provided by J. Mielke, A. Saywell, and L. Grill. Data acquired at the Fritz-Haber Institut of the Max Planck Society, Berlin (unpublished).

[30] P. Havu, V. Blum, V. Havu, P. Rinke, and M. Scheffler, Phys. Rev. B **82**, 161418(R) (2010).

[31] Y. Wang, N. S. Hush, and J. R. Reimers, Phys. Rev. B **75**, 233416 (2007).

[32] F. Ercolessi, A. Bartolini, M. Garofalo, M. Parrinello, and E. Tosatti, Surf. Sci. **189**, 636 (1987).

[33] F. Ercolessi, M. Parrinello, and E. Tosatti, Philos. Mag. A **58**, 213 (1988).

[34] M. Mansfield and R. J. Needs, J. Phys.: Condens. Matter **2**, 2361 (1990).

[35] N. Takeuchi, C. T. Chan, and K. M. Ho, Phys. Rev. B **43**, 13899 (1991).

[36] G. Kresse and J. Furthmüller, Phys. Rev. B **54**, 11169 (1996).

[37] G. Kresse and D. Joubert, Phys. Rev. B **59**, 1758 (1999).

[38] M. Dion, H. Rydberg, E. Schroder, D. C. Langreth, and B. I. Lundqvist, Phys. Rev. Lett. **92**, 246401 (2004).

[39] J. Klimeš, D. R. Bowler, and A. Michaelides, Phys. Rev. B **83**, 195131 (2011).

[40] J. P. Perdew, K. Burke, and M. Ernzerhof, Phys. Rev. Lett. **77**, 3865 (1996).

[41] M. Mura, A. Gulans, T. Thonhauser, and L. Kantorovich, Phys. Chem. Chem. Phys. **12**, 4759 (2010).

[42] J. Carrasco, B. Santra, J. Klimeš, and A. Michaelides, Phys. Rev. Lett. **106**, 026101 (2011).

[43] P. V. C. Medeiros, G. K. Gueorguiev, and S. Stafström, Phys. Rev. B **85**, 205423 (2012).

[44] R. Peköz, K. Johnston, and D. Donadio, J. Phys. Chem. C **116**, 20409 (2012).

[45] G. Li, I. Tamblyn, V. R. Cooper, H.-J. Gao, and J. B. Neaton, Phys. Rev. B **85**, 121409(R) (2012).

[46] J. Carrasco, J. Klimeš, and A. Michaelides, J. Chem. Phys. **138**, 024708 (2013).

[47] See Supplemental Material at http://link.aps.org/supplemental/10.1103/PhysRevB.87.235422 for additional results involving the PBE density functional, additional density of states plots, and optimized coordinates of the Au $22 \times \sqrt{3}$ cell.

[48] B. Hammer and M. Scheffler, Phys. Rev. Lett. **74**, 3487 (1995).

[49] A. Roudgar and A. Groß, Phys. Rev. B **67**, 033409 (2003).

[50] B. Hammer and J. K. Nørskov, Surf. Sci. **343**, 211 (1995).